Journal of Physics and Chemistry of Solids 134 (2019) 324–332

Contents lists available at ScienceDirect

Journal of Physics and Chemistry of Solids

journal homepage: www.elsevier.com/locate/jpcs

The role of strong electron correlations in determination of band structure and charge distribution of transition metal dihalide monolayers

E.A. Kovaleva[a,b,*], Iuliia Melchakova[a,b], N.S. Mikhaleva[a], F.N. Tomilin[a,c], S.G. Ovchinnikov[a,c], Woohyeon Baek[b], V.A. Pomogaev[d], P. Avramov[b,**], A.A. Kuzubov[1]

[a] Siberian Federal University, 79 Svobodny Pr., Krasnoyarsk, 660041, Russia
[b] Kyungpook National University, 80 Daehakro, Bukgu, Daegu, 41566, South Korea
[c] Kirensky Institute of Physics, FRC KSC SB RAS, 50 Academgorodok, Krasnoyarsk, 660036, Russia
[d] Tomsk State University, 36 Lenin Prospekt, Tomsk, 634050, Russian Federation

ARTICLE INFO

The authors dedicate this article to the memory of Prof. Alexander A. Kuzubov as he was the one who originally inspired this work but deceased before we could finish it.

Keywords:
Transition metal dihalides
Monolayers
DFT
Hubbard correction
Band structure

ABSTRACT

Electronic structure and magnetic properties of the family of first-row transition metal dihalides (TMHal_2, TM = V, Cr, Mn, Fe, Co, Ni; H = Br, I) monolayers were studied by means of density functional theory. Strong electron correlations were taken into account by implementing Hubbard U correction in a simplified scheme proposed by Dudarev et al. (U_{eff}). U_{eff} correction essentially affects electronic structure of TMHal_2 widening the band gap and witnessing their highly spin-polarized nature. Two different ligand orientations namely, H and T configurations of monolayers were considered. Unlike others, FeHal_2 monolayers tend to form H structure when U_{eff} correction is included.

1. Introduction

Since the discovery of free-standing graphene [1,2], two-dimensional materials have attracted lots of attention due to their unusual mechanical and electronic properties being rather different from those of the bulk material. In particular, they are being considered as promising materials for spintronics. The use of low-dimensional materials allows decreasing the size of spintronic devices essentially. However, the utilization of graphene in spintronic devices is limited due to its conducting semi-metal nature while contemporary tasks often require a semiconducting or half-metallic material. Along with tuning graphene properties by various methods, new 2D layered materials are developed. Transition metal dichalcogenides (TMD) are of a particular interest because of the wide variety of their electronic properties which enables one to use them in opto- and nanoelectronics [3]. The most studied among all the TMD monolayers are MoX_2 and WX_2 (X = S, Se), or so-called MoWSeS materials [4]. However, to the date, vast majority of TMD family does not possess magnetic ordering. The only exceptions are VS_2 and VSe_2 which appear to be surprisingly intrinsic ferromagnets [5–7]. It's worth to note that TMD monolayers are actually not atomically thin but represent a three-layered structure with metal ions being sandwiched between two chalcogen's layers. There are, then, two possible configurations of layers mutual arrangement, namely, H (hexagonal, with metal in trigonal prismatic surrounding) and T (trigonal, with metal in octahedral surrounding). It was shown by density functional calculations that quantum confinement effect plays a key role in stabilization of monolayer structure. Even though bulk VS_2 has T structure and keeps it when going to the bilayer, H configuration is more favorable for its monolayer [7]. This, in turn, affects monolayer's properties strongly, particularly magnetic ordering. The strain dependence of magnetism in VX_2 (X = S, Se) was explained by Ma et al. as the complex interplay between covalent and ionic bonding [5]. There are several studies aimed to modulate magnetic properties of TMD monolayers by strain, functionalization of the material or their combination [8,9].

Transition metal dihalides ($TMHal_2$) are substantially less investigated though being structurally analogous to TMD family in terms of the monolayer structure. Up to the date, $TMHal_2$ monolayers have

* Corresponding author. 79 Svobodny pr., Siberian Federal University, Research Department, Krasnoyarsk, 660041, Russia.
** Corresponding author.
E-mail addresses: kovaleva.evgeniya1991@mail.ru (E.A. Kovaleva), paul.veniaminovich@knu.ac.kr (P. Avramov).
[1] Deceased 12/31/2016.

https://doi.org/10.1016/j.jpcs.2019.05.036
Received 21 August 2018; Received in revised form 6 December 2018; Accepted 24 May 2019
Available online 29 May 2019
0022-3697/

Table 1
Effective U_{eff} values for the first-row transition metal compounds [36].

	V	Cr	Mn	Fe	Co	Ni
U_{eff}, eV	3.1	3.5	4.0	4.0	3.3	6.4

not been obtained yet, though there are some reports of PbI_2 monolayer preparation by ion intercalation [10]. Fast development of two-dimensional materials synthesis methods such as liquid exfoliation assisted by surfactants or polymers [11] makes it reasonable to expect $TMHal_2$ monolayers to be obtained in the nearest future. Along with that, one can expect them to possess challenging magnetic properties due to both larger degree of ionic bonding and expected complex magnetic ordering [12]. However, only a few theoretical studies of their electronic structure can be found [13,14]. Some spin polarization was reported for several compounds, namely, vanadium, cobalt, nickel dihalides [14]. Previously, properties of $TMHal_2$ were investigated in T-structure only while, as was shown [7], H structure can be stable as well even if not existing in the bulk.

According to the literature, all first-row TMI_2 (TM = V, Cr, Mn, Fe, Co, Ni) compounds are antiferromagnets [15–17]. Most of $TMHal_2$ possess CdI_2-type structure (so-called 1T structure, P-3m1 space group), except of $NiHal_2$ obeying $CdCl_2$-type structure (3T structure with ABC stacking of both nickel and halide ions, R-3m:H space group) [18] and $CrHal_2$, for which both orthorhombic (Cmc21) [19] and pseudo-hexagonal monoclinic (C2/m) [20] structures are reported. Friedt et al. [21] reported the simplest antiferromagnetic structure compatible with the Mössbauer spectroscopy results for VI_2, CoI_2, NiI_2 to be A-type antiferromagnetic phase with spins aligned along the metal to iodine bonds while FeI_2 is proposed to be DF-type antiferromagnet [21,22]. This magnetic structure is similar to that of $MnBr_2$ [23] but magnetic moments are parallel to c axis and perpendicular to Fe layers. Magnetic unit cell of FeI_2 is 16 times larger than crystallographic unit cell. According to the neutron diffraction data, MnI_2 possesses helical antiferromagnetic ordering with moments ferromagnetically aligned in (307) planes and rotated by $2\pi/16$ in subsequent sixteen (307) planes [24].

The present work is aimed to study the role of strong electron correlations in determination of the main features of electronic and magnetic properties of the first-row transition metal dihalides $TMHal_2$ (TM = 3d metal, Hal = Br, I) using GGA + U calculations. For the sake of comparison, the conventional GGA-PBE approach was used as a reference.

2. Computational methods

All calculations were performed within the framework of density functional theory using PBE exchange-correlation functional [25,26] and projector augmented wave method [27,28], as implemented in Vienna Ab-initio Simulation Package [29–32]. Grimme D3 correction [33] was used to describe van-der-Waals interactions between $TMHal_2$ layers. In order to account the correlation effects which are usually significant in transition metal compounds, the simplified form of Hubbard U correction proposed by Dudarev et al. [34,35] was implemented. Effective U parameters (U_{eff} = U - J, where U stands for the Coulomb repulsion and J is the exchange parameter) for TM atoms were adopted from Wang et al. [36].

First, unit cell optimization of transition method dihalides (TM = V, Cr, Mn, Fe, Co, Ni; Hal = Br, I) was performed. Then, monolayers were cut from the initial structures along the (001) surface. Two different configurations of $TMHal_2$ monolayers were considered, namely, H (trigonal prismatic) and T (octahedral) ones (see Fig. 1). In fact, first-layer ligand atoms in T configuration are rotated by 60° with respect to the second-layer atoms while both first and second ligand layers have the same orientation for H configuration.

The Mönkhorst-Pack [37] scheme was implemented for k-point Brillouin zone sampling. 9 × 9 × 1 *k*-point mesh was used for $NiBr_2$, NiI_2 bulk unit cells possessing 3T structure while 9 × 9 × 3 grid was used for bulk calculation of other compounds with 1T structure. A vacuum interval of 20 Å was set normal to the monolayer plane in order to avoid artificial interactions in periodic boundary conditions. *k*-point grid contained 9 × 9 × 1 points for all monolayer structures. Stopping criterion for the geometry optimization was the force acting on atoms less than 0.001 eV/Å. For the sake of comparison, formation energy of different $TMHal_2$ structures per formula unit was calculated as

$$E = E_{ML}/n_1 - E_{UC}/n_2$$

E_{ML} and E_{UC} stand for total energies of the monolayer and corresponding bulk unit cell, n_1 and n_2 stand for the number of formula units per monolayer and bulk unit cell, respectively.

Phonon spectra were calculated as an indicator of stability and the structures with 3 or less small negative modes which have purely computational origin were considered to be stable (see Figs. 1S-12S in SI). In order to verify structural stability of planar 2D TM halide materials against bending due to internal mechanical stress [38], a set of additional calculations of halide 3 × 3 clusters was performed. Neighboring images were distinguished from each other by 10 Å of vacuum in each direction in order to prevent artificial interactions in periodic boundary conditions. Structures are considered as stable as they do not

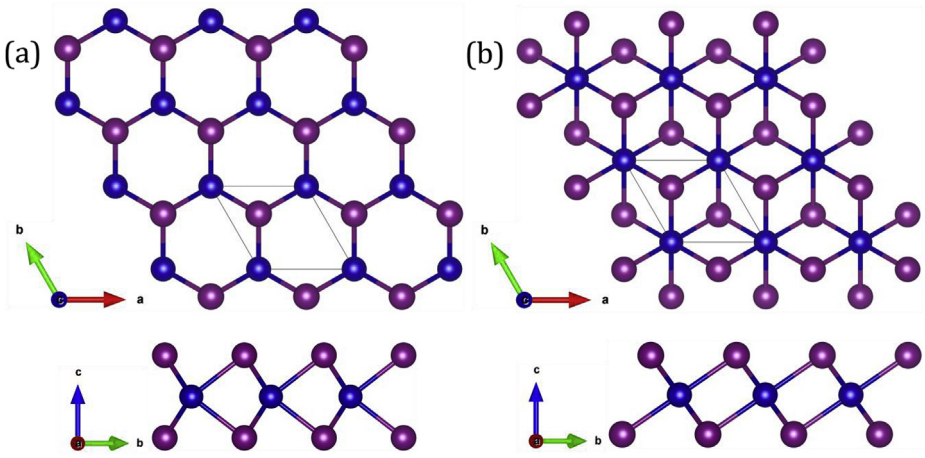

Fig. 1. Structures of (a) H and (b) T configurations of $TMHal_2$ monolayers. TM ions are presented in dark blue, halide ions are presented in purple. Black rhombus demonstrates the top view of monolayer unit cell.

Table 2
Structural parameters of $TMHal_2$ structures.

Compound	Structure	Unit cell structural parameters, Å (Metal-ligand bond distance, Å)			Formation energy, eV/formula unit	
		PBE + U	PBE	Experiment	PBE + U	PBE
VBr_2	Bulk (P-3 m1)	a = b = 3.83, c = 6.05 (2.66)	a = b = 3.82, c = 6.09 (2.63)	a = b = 3.75, c = 6.20 [39] (no data)	0.00	0.00
	H monolayer	a = b = 3.70	a = b = 3.61	–	1.02	1.04
	T monolayer	a = b = 3.85	a = b = 3.80	–	0.17	0.17
$CrBr_2$	Bulk (C2/m)	a = 6.51 b = 3.94 c = 6.10 (2.76; 2.56)	a = 6.61 b = 3.75, c = 5.98 (2.70; 2.61)	a = 7.11; b = 3.64; c = 6.24 (2.99; 2.55) [40]	0.00	0.00
	H monolayer	a = b = 3.71	a = b = 3.66	–	1.12	0.79
	T monolayer	a = b = 3.82	a = b = 3.79	–	0.66	0.31
$MnBr_2$	Bulk (P-3 m1)	a = b = 3.88, c = 6.27 (2.72)	a = b = 3.86, c = 6.38 (2.69)	a = b = 3.82, c = 6.19 (2.69) [18]	0.00	0.00
	H monolayer	a = b = 3.76	a = b = 3.70	–	0.60	0.57
	T monolayer	a = b = 3.89	a = b = 3.87	–	0.17	0.35
$FeBr_2$	Bulk (P-3 m1)	a = b = 3.88, c = 6.27 (2.64)	a = b = 3.71, c = 6.24 (2.62)	a = b = 3.78, c = 6.22 (2.64) [41]	0.00	0.00
	H monolayer	a = b = 3.65	a = b = 3.55	–	0.01	0.40
	T monolayer	a = b = 3.75	a = b = 3.70	–	0.18	0.18
$CoBr_2$	Bulk (P-3 m1)	a = b = 3.75, c = 6.14 (2.61)	a = b = 3.67, c = 6.08 (2.57)	a = b = 3.68, c = 6.12 (2.62) [18]	0.00	0.00
	H monolayer	a = b = 3.58	a = b = 3.55	–	1.26	0.62
	T monolayer	a = b = 3.74	a = b = 3.67	–	0.17	0.22
$NiBr_2$	Bulk (R-3 m:H)	a = b = 3.68, c = 18.58 (2.58)	a = b = 3.66, c = 18.10 (2.63)	a = b = 3.71, c = 18.3 (2.58) [18]	0.00	0.00
	H monolayer	a = b = 3.41	a = b = 3.56	–	1.11	1.00
	T monolayer	a = b = 3.68	a = b = 3.66	–	0.16	0.17
VI_2	Bulk (P-3 m1)	a = b = 4.13. c = 6.73 (2.89)	a = b = 4.10 c = 6.15 (2.82)	a = b = 4.02, c = 6.71 [39] (no data)	0.00	0.00
	H monolayer	a = b = 3.71	a = b = 3.93	–	0.86	1.18
	T monolayer	a = b = 3.88	a = b = 4.07	–	0.02	0.84
CrI_2	Bulk (C2/m)	a = 6.99 b = 4.19, c = 8.28 (2.78; 2.97)	a = 7.09 b = 4.00, c = 7.80 (2.78; 3.01)	a = 7.55; b = 3.93; c = 7.51 (2.74; 3.24) [20]	0.00	0.00
	H monolayer	a = b = 3.95	a = b = 3.89	–	0.79	0.71
	T monolayer	a = b = 4.05	a = b = 4.02	–	0.35	0.23
MnI_2	Bulk (P-3 m1)	a = b = 4.15, c = 6.84 (2.93)	a = b = 4.10, c = 6.81 (2.89)	a = b = 4.16, c = 6.82 (2.95) [18]	0.00	0.00
	H monolayer	a = b = 4.06	a = b = 3.99	–	0.63	0.62
	T monolayer	a = b = 4.16	a = b = 4.10	–	0.20	0.20
FeI_2	Bulk (P-3 m1)	a = b = 4.04, c = 6.77 (2.85)	a = b = 3.98, c = 6.72 (2.81)	a = b = 4.04, c = 6.75 (2.88) [18]	0.00	0.00
	H monolayer	a = b = 3.96	a = b = 3.84	–	0.10	0.50
	T monolayer	a = b = 4.04	a = b = 3.99	–	0.20	0.21
CoI_2	Bulk (P-3 m1)	a = b = 4.03, c = 6.63 (2.81)	a = b = 3.94, c = 6.58 (2.76)	a = b = 3.96, c = 6.65 (2.83) [18]	0.00	0.00
	H monolayer	a = b = 3.87	a = b = 3.82	–	1.25	0.69
	T monolayer	a = b = 4.04	a = b = 3.94	–	0.19	0.29
NiI_2	Bulk (R-3 m:H)	a = b = 3.98, c = 20.10 (2.78)	a = b = 3.91, c = 19.41 (2.72)	a = b = 3.89, c = 19.63 (2.78) [18]	0.00	0.00
	H monolayer	a = b = 3.92	a = b = 3.81	–	1.06	0.96
	T monolayer	a = b = 3.75	a = b = 3.93	–	0.19	0.20

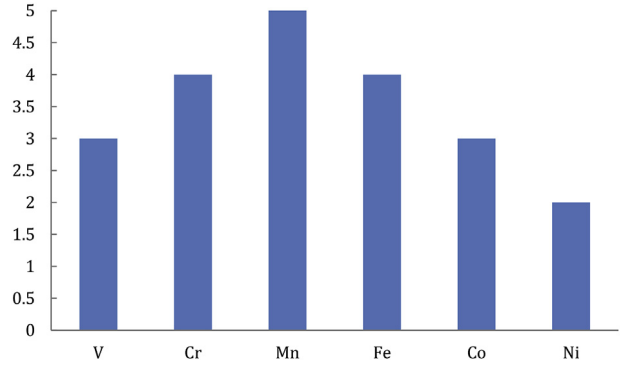

Fig. 2. Magnetic moments on TM ions in $TMHal_2$ monolayers. PBE and PBE + U results coincide up to 0.01 μ_B for both TM bromides and iodides.

twist and retain their planar geometry during the optimization process (see Fig. 13S).

3. Results and discussion

3.1. Structural parameters

Unit cell parameters and formation energy values for $TMHal_2$ structures are summarized in Table 2. Structural parameters obtained for bulk $TMHal_2$ compounds are in good agreement with experimental values [18,20,39–41]. It's worth noting that PBE + U method gives slightly larger values of the cell vectors than pure PBE does. Anyway, it shows more accurate values of the lengths of metal-ligand bonds [18,20,39–41] in these compounds.

At PBE level of theory, T configuration of monolayer is energetically favorable in all cases, in conformity with the fact that bulk materials

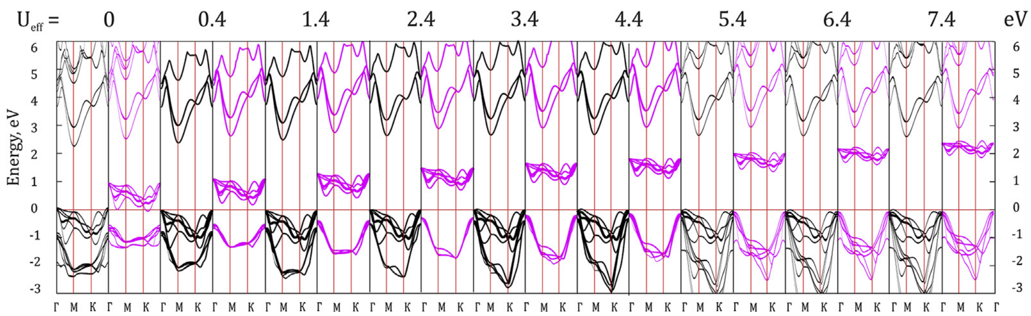

Fig. 3. Dependence of NiI_2 band structure on the value of U_{eff} parameter. At $U_{eff} = 0$ eV PBE + U approach is equivalent to PBE. Increasing of U_{eff} leads to visible increase of spin-down band gap. At $U_{eff} = 6.4$ eV and higher the spin-down band gap stays virtually the same and approximately equal to 1.80 eV. Black and purple lines correspond to spin-up and spin-down states, respectively.

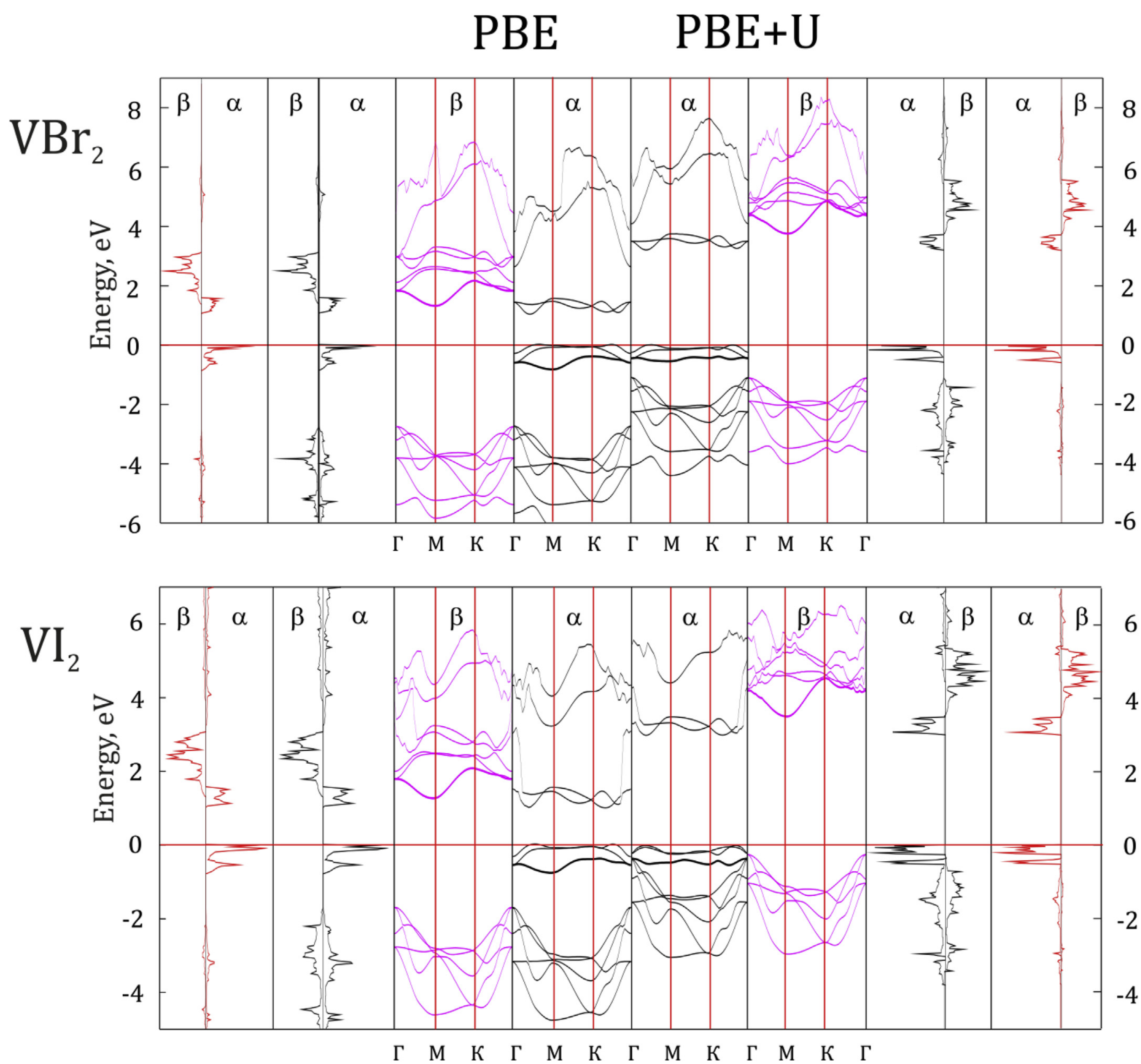

Fig. 4. PBE (left) and PBE + U (right) spin-resolved band structures, TDOS (black lines) and vanadium ion PDOS (red lines) of VBr_2 (top) and VI_2 (bottom).

adopt this structure as well. At GGA + U level of theory, the only exceptions are $FeBr_2$ and FeI_2 with H configuration favorable with a minor difference of ~0.1 eV per formula unit between H and T configurations. The value of U_{eff} correction strongly affects the stability of H structure in $FeHal_2$. A set of additional test calculations was performed to find the U_{eff} value threshold for the inversion of T/H structure stability. All U_{eff} values less than 4.0 eV as well as combinations with non-zero J value (J = 1.0 eV) result in stable T configuration. The

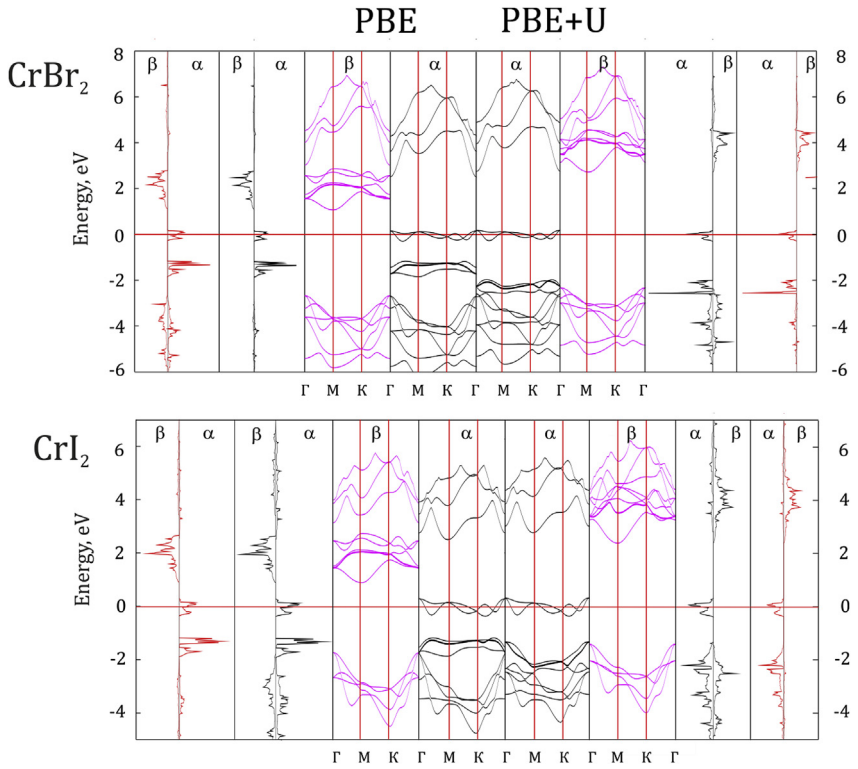

Fig. 5. PBE (left) and PBE + U (right) spin-resolved band structures, TDOS (black lines) and chromium ion PDOS (red lines) of $CrBr_2$ (top) and CrI_2 (bottom).

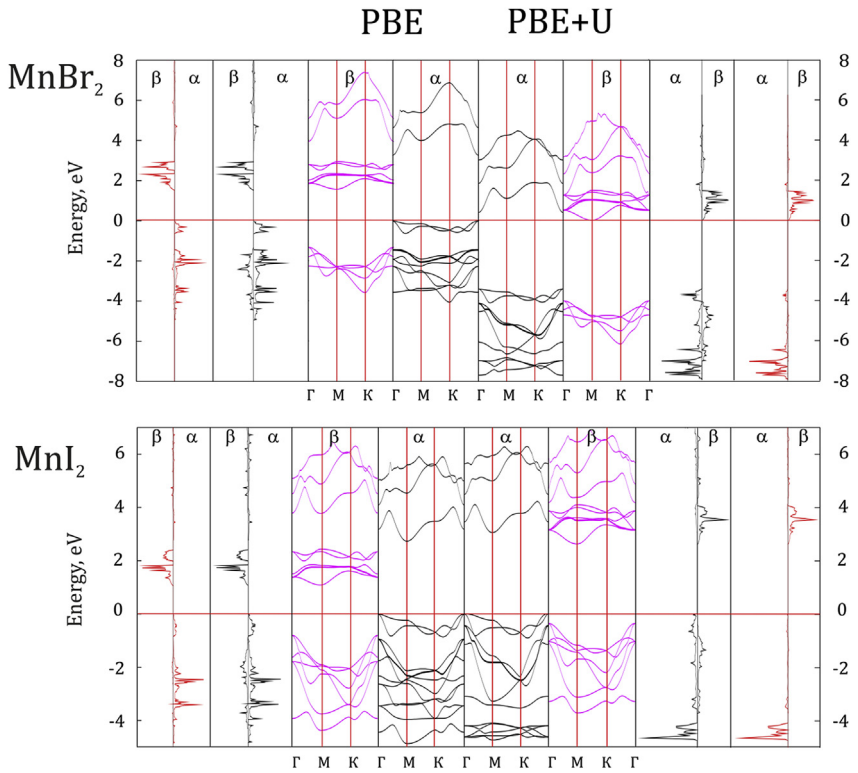

Fig. 6. PBE (left) and PBE + U (right) spin-resolved band structures, TDOS (black lines) and manganese ion PDOS (red lines) of $MnBr_2$ (top) and MnI_2 (bottom).

same effect was previously shown for some TMDs [3,7]. In order to prove our choice of U, additional test electronic structure calculations of $FeCl_2$ T monolayer were carried out. This structure was previously investigated by Torun et al. [42] using GGA-PBE and hybrid HSE06 functionals and found to be half-metallic with spin-down band gap of 4.4 (PBE) or 6.7 (HSE06) eV. We performed band structure calculation of $FeCl_2$ using GGA-PBE with the effective Hubbard correction of 4 eV and found the spin-down band gap width (~6.3 eV, see below) to be in a good agreement with HSE06 functional (see Fig. 14S in SI).

Formation energies of favorable monolayer configurations are

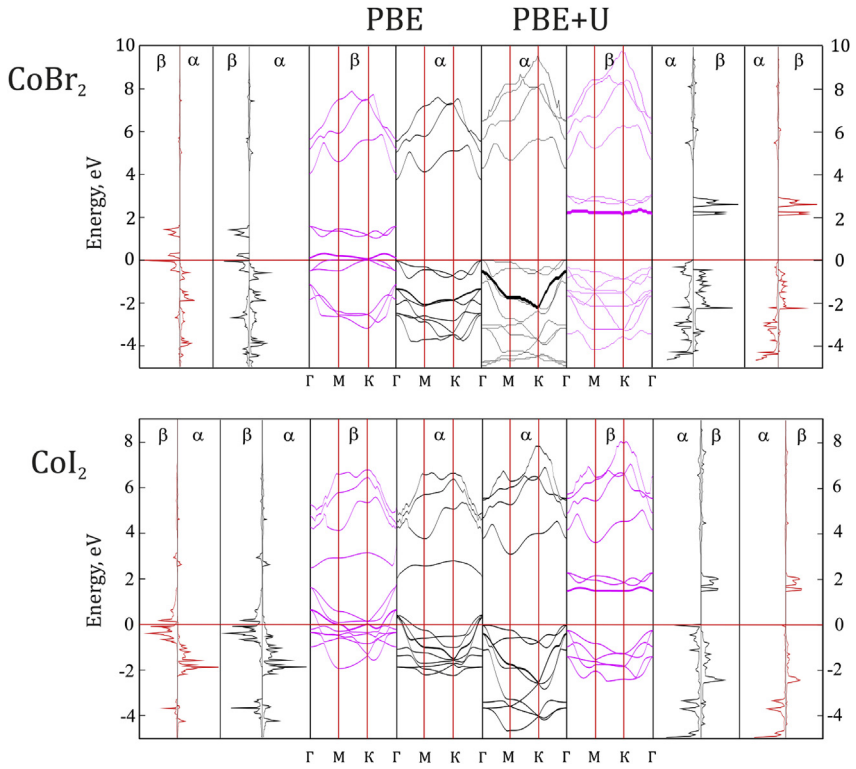

Fig. 7. PBE (left) and PBE + U (right) spin-resolved band structure, TDOS (black lines) and cobalt ion PDOS (red lines) of $CoBr_2$ (top) and CoI_2 (bottom).

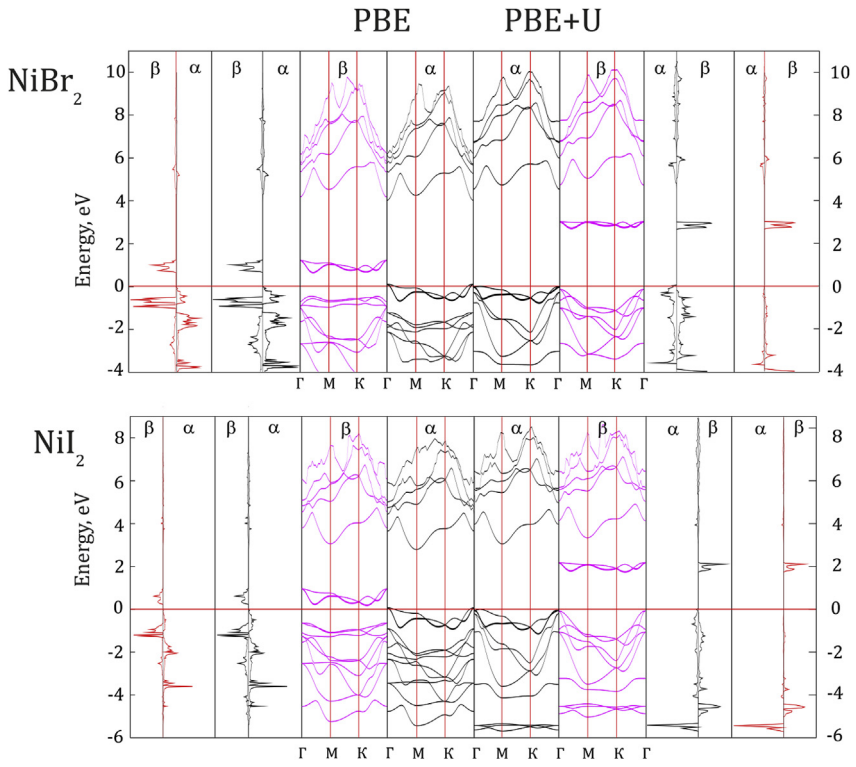

Fig. 8. PBE (left) and PBE + U (right) spin-resolved band structures, TDOS (black lines) and nickel ion PDOS (red lines) of $NiBr_2$ (top) and NiI_2 (bottom).

considerably small, confirming van-der-Waals character of bonding between adjacent layers in the bulk and assuring of the possibility of monolayers experimental synthesis (Table 2).

3.2. Electronic and magnetic properties of 2D transition metal dihalides

Since Br^- and I^- anions are known to be weak field ligands, d-orbitals of TM ions are not expected to split much and so the high-spin state is likely to occur which means that $TMHal_2$ compounds should possess magnetic moment on the metal ions. In agreement with

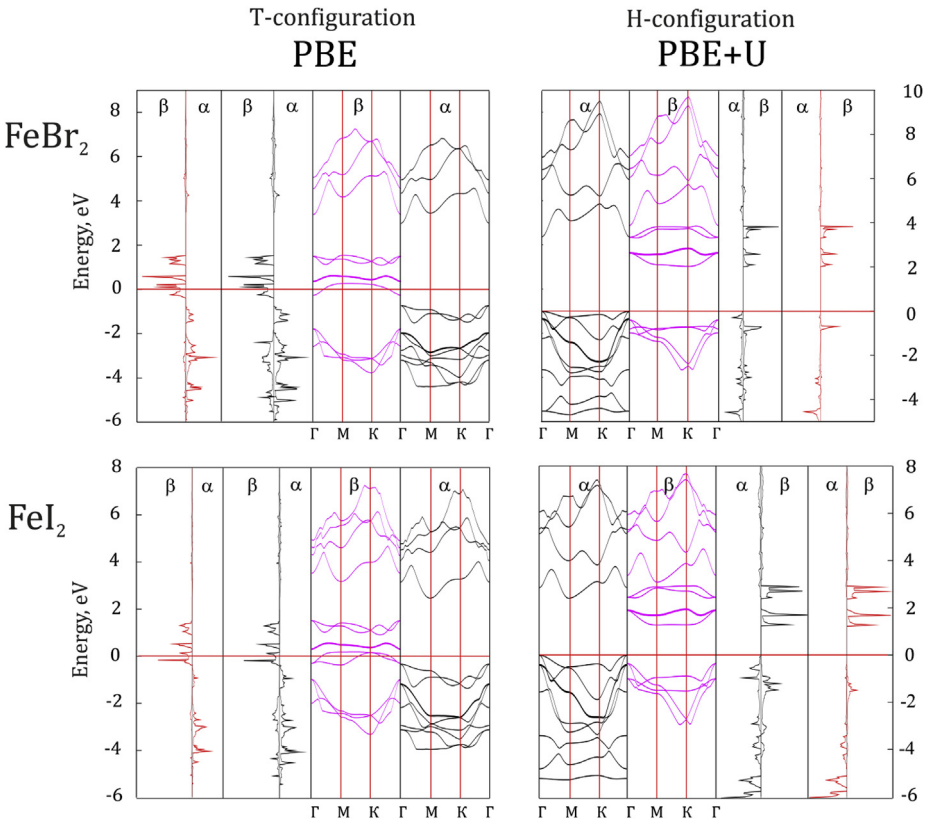

Fig. 9. PBE (left) and PBE + U (right) spin-resolved band structures, TDOS (black lines) and nickel ion PDOS (red lines) of $FeBr_2$ (top) and FeI_2 (bottom).

Table 3
Band gaps for energetically favorable TM*Hal*$_2$ monolayers. Direct and indirect gaps are denoted as (d) and (i), respectively.

TM*Hal*$_2$ structure	Band gap (PBE + U)	Band gap (PBE)
VBr_2 T	3.10 (i)	1.10 (i)
$CrBr_2$ T	half-metal	half-metal
$MnBr_2$ T	3.70 (i)	1.50 (i)
$FeBr_2$ T	–	half-metal
$FeBr_2$ H	2.00 (i)	–
$CoBr_2$ T	2.30 (d)	spin-gapless
$NiBr_2$ T	2.50 (i)	0.70 (i)
VI_2 T	3.00 (i)	1.00 (i)
CrI_2 T	half-metal	half-metal
MnI_2 T	2.50 (i)	1.00 (i)
FeI_2 T	–	1.20 (i)
CoI_2 T	1.50 (d)	metal
NiI_2 T	1.80 (i)	1.15 (i)

previous theoretical results [13,14], both PBE and PBE + U methods show large magnetic moments localized on TM ions for all structures under consideration (see Fig. 2).

Then, electronic structures of TM*Hal*$_2$ monolayers were analyzed. Effective U_{eff} parameter for Ni ion proposed by Wang et al. [36] is noticeably larger than for the other TM ions (see Table 1). In order to check the validity of this value, a series of additional band structure calculations with different U_{eff} was performed for NiI_2 bulk unit cell. Fig. 3 illustrates the change in electronic structure with the increase of U_{eff}.

Ten different values of U_{eff} were tested, namely, 0.0 (corresponding to the conventional PBE); 0.4; 1.4; 2.4; 3.4; 4.4; 5.4; 6.4; 7.4 eV. As U_{eff} increases from 0.0 to 5.4 eV, the spin-down conduction band edge moves up from the Fermi level so NiI_2 changes its nature from spin-gapless semiconductor [43,44] to the ordinary spin-polarized semiconducting material. Spin-down valence band shifts to higher energies as well, almost approaching the Fermi level when U_{eff} = 7.4 eV. Highest occupied spin-up band lies close to the Fermi level without crossing it, spin-up band gap doesn't change as U_{eff} increases. Spin-down band gap

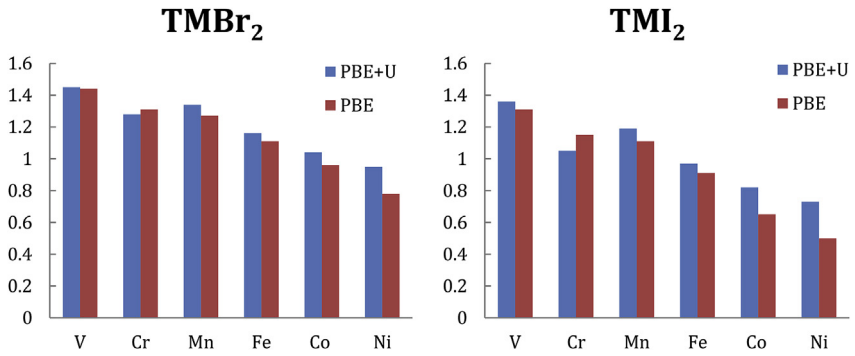

Fig. 10. Atomic charges of TM ions in TM*Hal*$_2$ compounds.

remains virtually the same (1.80 eV) for U_{eff} = 6.4 eV and higher. Hence, keeping in mind the absence of experimental data, U_{eff} = 6.4 eV [36] was used for further calculations.

Figs. 4–9 show band structures, total (TDOS) and partial (PDOS) densities of states for energetically favorable TM*Hal*$_2$ configurations. It can be clearly seen that Hubbard correction influences electronic properties of structures under investigation drastically.

For both VBr_2 and VI_2 U_{eff} correction enlarges the spin-up band gap without changing their semiconducting nature (~1 eV and ~3 eV, respectively) (see Fig. 4). Oppositely, only spin-down channel of chromium dihalides is affected when implementing Hubbard correction. Both $CrBr_2$ and CrI_2 demonstrate large spin-down band gap along with half-filled states crossing the Fermi level in spin-up channel revealing their half-metallic nature (Fig. 5). $MnBr_2$ monolayer is more complex in these terms. Introduction of U_{eff} parameter not only changes the width of spin-down gap but also shifts the whole spin-up channel down in energy by ~3 eV (Fig. 6). This doesn't happen for MnI_2 which is more similar to chromium compounds: spin-down band gap becomes larger while spin-up channel is practically intact.

Introduction of non-zero U_{eff} correction changes the electronic properties of cobalt dihalides drastically (Fig. 7). At PBE level of theory, $CoBr_2$ has typical spin-gapless band structure with large spin-up band gap (4.10 eV), and CoI_2 is metallic. Introduction of Hubbard correction leads to significant shift of both valence and conduction band edges resulting in semiconducting $CoHal_2$ band structures.

At PBE + U level of theory the nickel halide spin-down band gaps are almost twice larger than the PBE ones while spin-up electronic subsystems are virtually intact (Fig. 8). Both $NiBr_2$ and NiI_2 are spin-polarized semiconductors.

Iron dihalides are kind of exception since including of U_{eff} correction leads to the inversion of energetically favorable configuration. While T-configuration (PBE level of theory) demonstrates half-metallic behavior for both $FeBr_2$ and FeI_2, the H-configuration monolayers (PBE + U method) are spin-polarized semiconductors (Fig. 9).

For all semiconducting compounds, except of $MnBr_2$, the top of the valence band reaches the Fermi level while $MnBr_2$ demonstrates conduction band touching the Fermi level. This opens a possibility to tune their properties by inducing point defects or doping and easily obtain half-metallic materials instead of semiconducting ones.

The values and characters of the TM*Hal*$_2$ band gaps are summarized in Table 3. Most of TM dihalides are indirect gap semiconductors. For them, introduction of U_{eff} correction enlarges the band gap without changing its indirect nature. Oppositely, cobalt halides monolayers demonstrate direct band gaps at PBE + U level of theory instead of metallic/spin-gapless band structure obtained by using PBE method.

Atomic charges of transition metal ions in TM*Hal*$_2$ 2D monolayers are presented in Fig. 10. Generally, the TM atomic charges decrease from V to Ni correlating with the decrease of the ionic size. Chromium dihalides are the exceptions of this trend which can be attributed to the high degree of structural deformation in comparison with their bulk counterparts which have pseudo-hexagonal monoclinic symmetry with distorted octahedral surrounding of Cr while the optimized 2D structures have six equidistant halide atoms around each chromium ion, similarly to the other structures having triangular symmetry of the bulk counterparts.

TM atomic charges in $TMBr_2$ are higher than in TMI_2, in agreement with bromine higher electronegativity. In general, PBE + U shows higher charges on TM ions, except of Cr. The difference between PBE and PBE + U results increases from V to Ni and from Br to I. However, the common trend can be clearly seen confirming the validity of PBE + U approach.

4. Conclusion

According to the results of PBE calculations, most of TM*Hal*$_2$ monolayers are semiconductors, except of metallic CoI_2, spin-gapless $CoBr_2$ and Cr*Hal*$_2$ which are half-metals. In general, introduction of Hubbard correction leads to the increase of the band gap. According to the results of PBE + U calculations, most of $TMHal_2$ monolayers are spin-polarized semiconductors, though there's an option of altering their properties to half-metallic. Chromium dihalides monolayers were found to be intrinsic half-metals. Inclusion of Hubbard U_{eff} correction enlarges the band gap, predominantly in one spin channel and may lead to the completely different electronic properties in comparison with pristine PBE. This effect is especially noticeable for Co-base compounds. In some cases, Hubbard correction can even lead to the inversion of favorable monolayer configuration, as was demonstrated for iron dihalides. Nevertheless, both methods give the same values of magnetic moments on metal atoms and the same trends for their partial charge dependence.

Acknowledgements

This work was supported by the government contract of the Ministry of Education and Science of the Russian Federation, Russia to Siberian Federal University (Grant No. 16.1455.2017/PCh) and Russian Foundation for Basic Research (RFBR), Russia (Grant No. 16-32-60003 mol_a_dk), Government of Krasnoyarsk Territory, Krasnoyarsk Regional Fund of Science to the research project: “Quantum chemical modeling of Bychkov-Rashba interfaces based on transition metal compounds and nanoscaled organic fragments” (Project No. 18-43-243011). The authors would like to thank Joint Supercomputer Center of RAS, Moscow; Center of Equipment for Joint Use of Siberian Federal University, Krasnoyarsk; and Information Technology Center, Novosibirsk State University for providing the access to their supercomputers. N.S.M. acknowledges the financial support of the RFBR, through the research project No. 16-32-60003 mol_a_dk. E.A. Kovaleva is grateful to the Foundation for Assistance to Small Innovative Enterprises (FASIE), Russia (Project no. 0033639). W.B. and P.A. gratefully acknowledge the financial support of National Research Foundation of Republic of Korea under the Grant No. NRF-2017R1A2B4004440.

Appendix A. Supplementary data

Supplementary data to this article can be found online at https://doi.org/10.1016/j.jpcs.2019.05.036.

References

[1] K.S. Novoselov, A.K. Geim, S.V. Morozov, D. Jiang, Y. Zhang, S. V Dubonos, I. V Grigorieva, A.A. Firsov, Electric field effect in atomically thin carbon films, Science 306 (2004) 666–669, https://doi.org/10.1126/science.1102896.
[2] K.S. Novoselov, A.K. Geim, S.V. Morozov, D. Jiang, M.I. Katsnelson, I.V. Grigorieva, S.V. Dubonos, A.A. Firsov, Two-dimensional gas of massless Dirac fermions in graphene, Nature 438 (2005) 197–200, https://doi.org/10.1038/nature04233.
[3] C. Ataca, H. Şahin, S. Ciraci, Stable, single-layer MX $_2$ transition-metal oxides and dichalcogenides in a honeycomb-like structure, J. Phys. Chem. C 116 (2012) 8983–8999, https://doi.org/10.1021/jp212558p.
[4] T. Heine, Transition metal chalcogenides: ultrathin inorganic materials with tunable electronic properties, Acc. Chem. Res. 48 (2015) 65–72, https://doi.org/10.1021/ar500277z.
[5] Y. Ma, Y. Dai, M. Guo, C. Niu, Y. Zhu, B. Huang, Evidence of the existence of magnetism in pristine VX $_2$ monolayers (X = S, Se) and their strain-induced tunable magnetic properties, ACS Nano 6 (2012) 1695–1701, https://doi.org/10.1021/nn204667z.
[6] H. Zhang, L.-M. Liu, W.-M. Lau, Dimension-dependent phase transition and magnetic properties of VS2, J. Mater. Chem. A. 1 (2013) 10821, https://doi.org/10.1039/c3ta12098h.
[7] A.H.M.A. Wasey, S. Chakrabarty, G.P. Das, Quantum size effects in layered VX $_2$ (X = S, Se) materials: manifestation of metal to semimetal or semiconductor transition, J. Appl. Phys. 117 (2015) 064313, , https://doi.org/10.1063/1.4908114.
[8] H. Shi, H. Pan, Y.-W. Zhang, B.I. Yakobson, Strong ferromagnetism in hydrogenated monolayer MoS 2 tuned by strain, Phys. Rev. B 88 (2013) 205305, https://doi.org/10.1103/PhysRevB.88.205305.
[9] H. Pan, Electronic and magnetic properties of vanadium dichalcogenides monolayers tuned by hydrogenation, J. Phys. Chem. C 118 (2014) 13248–13253, https://doi.org/10.1021/jp503030b.
[10] C.C. Coleman, H. Goldwhite, W. Tikkanen, A review of intercalation in heavy metal

iodides, Chem. Mater. 10 (1998) 2794–2800, https://doi.org/10.1021/cm980211r.
[11] V. Nicolosi, M. Chhowalla, M.G. Kanatzidis, M.S. Strano, J.N. Coleman, Liquid exfoliation of layered materials, Science 340 (2013) 1226419, https://doi.org/10.1126/science.1226419 (80-.).
[12] T. Kurumaji, S. Seki, S. Ishiwata, H. Murakawa, Y. Kaneko, Y. Tokura, Magnetoelectric responses induced by domain rearrangement and spin structural change in triangular-lattice helimagnets NiI 2 and CoI 2, Phys. Rev. B 87 (2013) 014429, , https://doi.org/10.1103/PhysRevB.87.014429.
[13] P. Miró, M. Audiffred, T. Heine, An atlas of two-dimensional materials, Chem. Soc. Rev. 43 (2014), https://doi.org/10.1039/C4CS00102H.
[14] S.-H. Lin, J.-L. Kuo, Towards the ionic limit of two-dimensional materials: monolayer alkaline earth and transition metal halides, Phys. Chem. Chem. Phys. 16 (2014) 20763–20771, https://doi.org/10.1039/C4CP02048K.
[15] B. Goodenough, Magnetism and Chemical Bond, New York (1963).
[16] W.E. Smith, Effects of antiferromagnetic coupling in the 5 k electronic spectra of crystals of vanadium dichloride, dibromide, and di-iodide, J. Chem. Soc. Dalton Trans. 0 (1972) 1634, https://doi.org/10.1039/dt9720001634.
[17] L.G. Van Uitert, H.J. Williams, R.C. Sherwood, J.J. Rubin, Graphical correlation of the néel temperatures of chlorides, bromides, and iodides of divalent 3 *d* transition metal ions, J. Appl. Phys. 36 (1965) 1029–1030, https://doi.org/10.1063/1.1714086.
[18] R.W.G. Wickoff, Crystal Structures, Interscience, New York, 1963.
[19] F. Besrest, S. Jaulmes, IUCr, Structure cristalline de l'iodure de chrome, CrI2, Acta Crystallogr. Sect. B Struct. Crystallogr. Cryst. Chem. 29 (1973) 1560–1563, https://doi.org/10.1107/S0567740873005030.
[20] J.W. Tracy, N.W. Gregory, J.M. Stewart, E.C. Lingafelter, The crystal structure of chromium(II) iodide, Acta Crystallogr. 15 (1962) 460–463, https://doi.org/10.1107/S0365110X62001152.
[21] J.M. Friedt, J.P. Sanchez, G.K. Shenoy, Electronic and magnetic properties of metal diiodides MI $_2$ (M = V, Cr, Mn, Fe, Co, Ni, and Cd) from ^{129} I Mössbauer spectroscopy, J. Chem. Phys. 65 (1976) 5093–5102, https://doi.org/10.1063/1.433072.
[22] J. Gelard, A.R. Fert, P. Meriel, Y. Allain, Magnetic structure of FeI2 by neutron diffraction experiments, Solid State Commun. 14 (1974) 187–189, https://doi.org/10.1016/0038-1098(74)90213-0.
[23] E.O. Wollan, W.C. Koehler, M.K. Wilkinson, Neutron diffraction study of the magnetic properties of Mn Br 2, Phys. Rev. 110 (1958) 638–646, https://doi.org/10.1103/PhysRev.110.638.
[24] J.W. Cable, M.K. Wilkinson, E.O. Wollan, W.C. Koehler, Neutron diffraction investigation of the magnetic order in Mn I 2, Phys. Rev. 125 (1962) 1860–1864, https://doi.org/10.1103/PhysRev.125.1860.
[25] J.P. Perdew, J.A. Chevary, S.H. Vosko, K.A. Jackson, M.R. Pederson, D.J. Singh, C. Fiolhais, Atoms, molecules, solids, and surfaces: applications of the generalized gradient approximation for exchange and correlation, Phys. Rev. B 46 (1992) 6671–6687, https://doi.org/10.1103/PhysRevB.46.6671.
[26] J.P. Perdew, J.A. Chevary, S.H. Vosko, K.A. Jackson, M.R. Pederson, D.J. Singh, C. Fiolhais, Erratum: atoms, molecules, solids, and surfaces: applications of the generalized gradient approximation for exchange and correlation, Phys. Rev. B 48 (1993) 4978, https://doi.org/10.1103/PhysRevB.48.4978.2.
[27] P.E. Blöchl, Projector augmented-wave method, Phys. Rev. B 50 (1994) 17953–17979, https://doi.org/10.1103/PhysRevB.50.17953.
[28] G. Kresse, D. Joubert, From ultrasoft pseudopotentials to the projector augmented-wave method, Phys. Rev. B 59 (1999) 1758–1775, https://doi.org/10.1103/PhysRevB.59.1758.
[29] G. Kresse, J. Furthmüller, Efficient iterative schemes for *ab initio* total-energy calculations using a plane-wave basis set, Phys. Rev. B 54 (1996) 11169–11186, https://doi.org/10.1103/PhysRevB.54.11169.
[30] G. Kresse, J. Furthmüller, Efficiency of ab-initio total energy calculations for metals and semiconductors using a plane-wave basis set, Comput. Mater. Sci. 6 (1996) 15–50, https://doi.org/10.1016/0927-0256(96)00008-0.
[31] G. Kresse, J. Hafner, *Ab initio* molecular-dynamics simulation of the liquid-metal–amorphous-semiconductor transition in germanium, Phys. Rev. B 49 (1994) 14251–14269, https://doi.org/10.1103/PhysRevB.49.14251.
[32] G. Kresse, J. Hafner, *Ab initio* molecular dynamics for liquid metals, Phys. Rev. B 47 (1993) 558–561, https://doi.org/10.1103/PhysRevB.47.558.
[33] S. Grimme, Semiempirical GGA-type density functional constructed with a long-range dispersion correction, J. Comput. Chem. 27 (2006) 1787–1799, https://doi.org/10.1002/jcc.20495.
[34] V.I. Anisimov, J. Zaanen, O.K. Andersen, Band theory and mott insulators: hubbard *U* instead of stoner *I*, Phys. Rev. B 44 (1991) 943–954, https://doi.org/10.1103/PhysRevB.44.943.
[35] S.L. Dudarev, G.A. Botton, S.Y. Savrasov, C.J. Humphreys, A.P. Sutton, Electron-energy-loss spectra and the structural stability of nickel oxide: An LSDA + U study, Phys. Rev. B 57 (1998) 1505–1509, https://doi.org/10.1103/PhysRevB.57.1505.
[36] L. Wang, T. Maxisch, G. Ceder, Oxidation energies of transition metal oxides within the GGA + U framework, Phys. Rev. B Condens. Matter 73 (2006) 1–6, https://doi.org/10.1103/PhysRevB.73.195107.
[37] H.J. Monkhorst, J.D. Pack, Special points for Brillouin-zone integrations, Phys. Rev. B 13 (1976) 5188–5192, https://doi.org/10.1103/PhysRevB.13.5188.
[38] P. Avramov, V. Demin, M. Luo, C.H. Choi, P.B. Sorokin, B. Yakobson, L. Chernozatonskii, Translation symmetry breakdown in low-dimensional lattices of pentagonal rings, J. Phys. Chem. Lett. 6 (2015) 4525–4531, https://doi.org/10.1021/acs.jpclett.5b02309.
[39] K. Hirakawa, H. Kadowaki, K. Ubukoshi, Study of frustration effects in two-dimensional triangular lattice antiferromagnets–neutron powder diffraction study of VX $_2$, X ≡ Cl, Br and I, J. Phys. Soc. Japan. 52 (1983) 1814–1824, https://doi.org/10.1143/JPSJ.52.1814.
[40] J.W. Tracy, N.W. Gregory, E.C. Lingafelter, IUCr, Crystal structure of chromium(II) bromide, Acta Crystallogr. 15 (1962) 672–674, https://doi.org/10.1107/S0365110X6200184X.
[41] J. Haberecht, H. Borrmann, R. Kniep, Refinement of the crystal structure of iron dibromide, FeBr2, Z. Kristallogr. N. Cryst. Struct. 216 (2001) 544, https://doi.org/10.1524/ncrs.2001.216.14.544.
[42] E. Torun, H. Sahin, S.K. Singh, F.M. Peeters, Stable half-metallic monolayers of FeCl $_2$, Appl. Phys. Lett. 106 (2015) 192404, https://doi.org/10.1063/1.4921096.
[43] X.L. Wang, Proposal for a new class of materials: spin gapless semiconductors, Phys. Rev. Lett. 100 (2008) 156404, https://doi.org/10.1103/PhysRevLett.100.156404.
[44] X.-L. Wang, S.X. Dou, C. Zhang, Zero-gap materials for future spintronics, electronics and optics, NPG Asia Mater. 2 (2010) 31–38, https://doi.org/10.1038/asiamat.2010.7.